

Extracting Light from Polymer Light-Emitting Diodes Using Stamped Bragg Gratings**

By Jonathan M. Ziebarth, Ameen K. Saafir, Shanhui Fan, and Michael D. McGehee*

In this paper, we describe a method for increasing the external efficiency of polymer light-emitting diodes (LEDs) by coupling out waveguided light with Bragg gratings. We numerically model the waveguide modes in a typical LED structure and demonstrate how optimizing layer thicknesses and reducing waveguide absorption can enhance the grating outcoupling. The gratings were created by a soft-lithography technique that minimizes changes to the conventional LED structure. Using one-dimensional and two-dimensional gratings, we were able to increase the forward-directed emission by 47 % and 70 %, respectively, and the external quantum efficiency by 15 % and 25 %.

1. Introduction

One of the most significant limitations on the external efficiency of polymer light-emitting diodes (LEDs) is waveguiding of light in the high-refractive-index active polymer and indium tin oxide (ITO) films. It has been estimated that more than half of the light generated in the active layer can be trapped inside the device.^[1] Approaches to solving this problem include microcavities that alter the directionality of emission,^[2,3] substrate modifications that enable extraction of light trapped in the substrate,^[4–8] and the introduction of periodic microstructures that outcouple trapped light from the organic/ITO layers.^[7,9–12] These methods have all shown promise, but the factors limiting light extraction and the effect of structure modification on device performance have not been completely examined. In this paper, we use both numerical and experimental techniques to explore Bragg gratings for outcoupling waveguided light and enhancing external efficiencies. We also demonstrate a soft-lithography technique for introducing Bragg gratings into polymer LEDs that could potentially be performed on a large scale at low cost.^[13]

2. Results and Discussion

2.1. Waveguiding and Light Scattering

The LED structure we chose to study is based on the polymer poly((2-methoxy-5-(3',7'-dimethyloctyloxy)-*para*-phenylenevinylene) (OC₁C₁₀-PPV).^[14] The chemical structure of this polymer and the most common LED structure are depicted in Figure 1. In this structure, carriers are injected from the ITO and calcium layers. The conducting polymer, poly(3,4-ethylenedioxythiophene)-poly(styrenesulfonate) (PEDOT-PSS) improves hole injection from the ITO. The silver layer serves as an encapsulating layer for the calcium.

During operation, a large fraction of the light generated in the polymer layer excites waveguide modes that travel along the active layer. Waveguide modes are described by their in-plane propagation vector, β , and the polarization of the electric field. Due to the highly anisotropic nature of OC₁C₁₀-PPV,^[15,16] practically all of the waveguided light has its electric field in the plane of the LED (transverse electric (TE)-polarized). Using the complex refractive indices of each layer,^[15,17,18] we have calculated the TE waveguide modes of OC₁C₁₀-PPV LEDs with 100 nm and 200 nm thick active layers. The effective indices of the modes are plotted in Figure 1c as a function of wavelength. As the active layer thickness increases, the in-plane propagation vector becomes larger. In Figure 2, we have plotted the calculated in-plane electric field profile for the TE₀ mode at $\lambda = 600$ nm for LEDs with 100 nm and 200 nm thick active layers. The fields were normalized so that the total (integrated) power in each structure was the same. The most obvious difference between the two structures is the location of the peak electric field. For a 100 nm thick film, the peak waveguide power is concentrated in the ITO layer, whereas in the 200 nm thick film, the peak power is located in the OC₁C₁₀-PPV layer. Also the peak field intensity is larger for the 200 nm thick device than the 100 nm thick device, and the mode is more confined in the light-emitting polymer.

[*] Prof. M. D. McGehee, J. M. Ziebarth, A. K. Saafir
Geballe Laboratory for Advanced Materials, Stanford University
Stanford, CA 94305 (USA)
E-Mail: mmcgehee@stanford.edu
Prof. S. Fan
Department of Electrical Engineering, Stanford University
Stanford, CA 94305 (USA)

[**] Financial support was provided by the National Science Foundation (ECS-0093502) and a DuPont Young Professor Award.

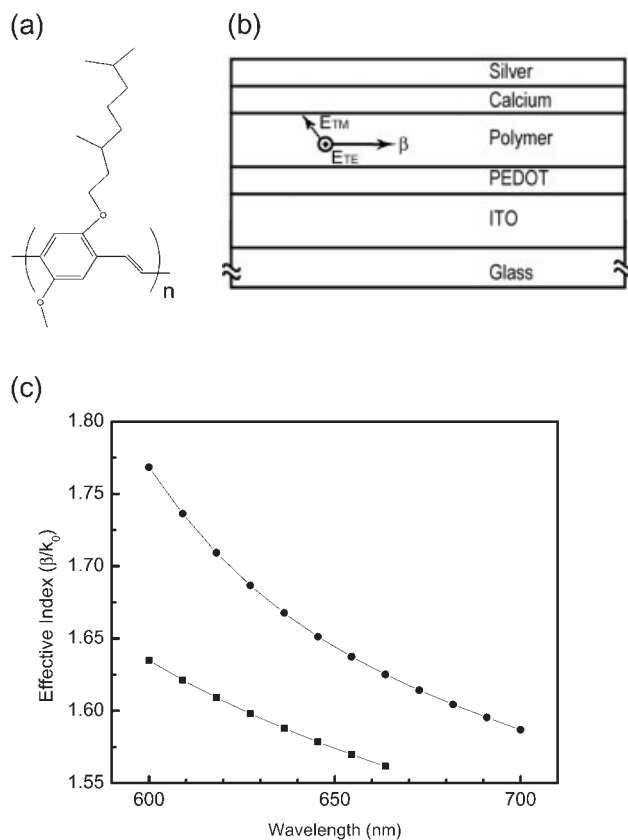


Figure 1. a) The chemical structure of OC₁C₁₀-PPV and b) the most common structure for LEDs made with this polymer. The reflection of light in the polymer layer can be represented by an in-plane wavevector β . The two possible electric field polarizations are also shown. c) The calculated waveguide modes versus wavelength for the LED structure in (b) for 100 nm thick (squares) and 200 nm thick (circles) active layer thicknesses. These modes are TE₀ modes, which are the lowest order modes where the electric field is entirely in the plane. The modes are written in terms of an effective index. The effective index is obtained by normalizing the in-plane propagation vector β by dividing by the free-space wavevector $k_0 = 2\pi/\lambda$.

By introducing a grating into this structure, the waveguided light can be coupled out of the device. The periodic variation in refractive index created by the grating introduces small reflections of the waveguided light. These reflections sum together over many periods and change the momentum of the waveguided light, allowing it to escape the LED. The angle of the outcoupled emission is given by

$$k_0 \sin \theta = \beta \pm (2\pi m/\Lambda) \quad (1)$$

where k_0 is the free-space wavevector of the scattered light, θ is the angle of emission with respect to normal, Λ is the grating period, and m is the scattering order. For the calculated mode values shown in Figure 1, first-order vertical outcoupling ($m=1$, $\theta=0^\circ$) requires gratings with periods between 350–450 nm.

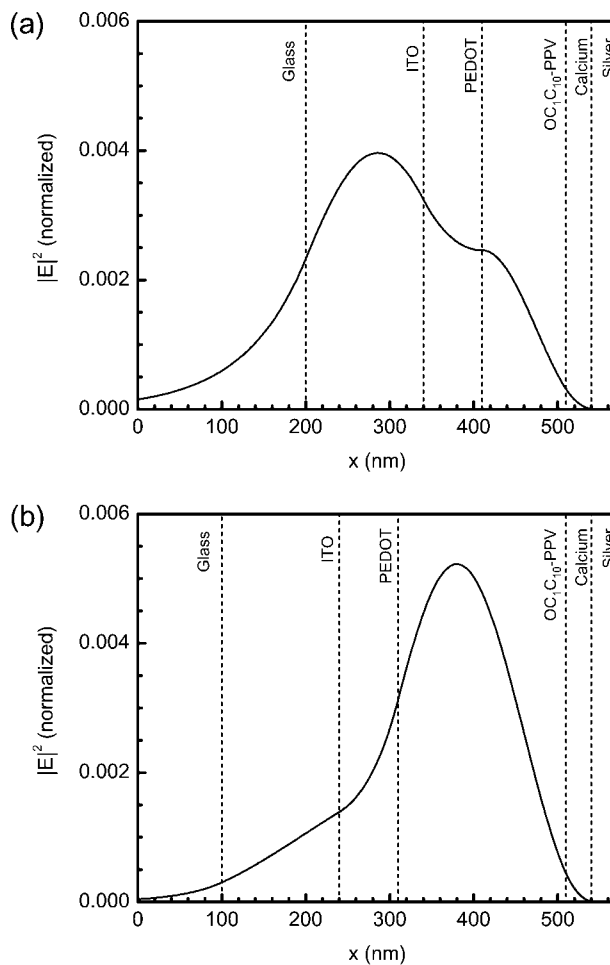


Figure 2. The distribution of the in-plane electric field intensity as a function of location for a) a 100 nm thick active layer and b) a 200 nm thick active layer. The fields have been normalized so that the intensity integrated over the depth is unity.

2.2. Grating Fabrication

To incorporate gratings into polymer LEDs with minimal change to device structure, cost, and fabrication, we patterned the PEDOT–PSS layer with a modified microtransfer molding technique.^[19] Holographic lithography was used to create Bragg grating templates with periods between 375–450 nm. A poly(dimethylsiloxane) (PDMS) prepolymer was poured over the templates and cured, producing a PDMS stamp with the same submicrometer features. A small (~10 μ L) drop of PEDOT–PSS was applied to a PDMS stamp with an area of 1 cm². The stamp was then applied to a glass substrate coated with a 140 nm thick ITO film. Gratings have been incorporated into other polymer films by similar techniques.^[19–22] However, most polymers are processed from hydrophobic solvents, while PEDOT–PSS is dispersed in water. Before stamping we treated

our ITO-coated glass substrates in a UV–ozone cleaner for 20 min. The PEDOT–PSS droplet beaded up on the hydrophobic PDMS stamp, but when the stamp and droplet were applied to the treated substrate, the drop quickly spread out, evenly coating the substrate. The stamp was then left on the substrate for several hours to allow the solvent to evaporate. The evaporation rate could be increased by using a thinner stamp or by heating the substrate during stamping. Finally, the stamp was removed to reveal the grating pattern in the PEDOT–PSS film. Figure 3 contains scanning electron microscopy (SEM) images of gratings in PEDOT–PSS produced by this technique. The depth of the gratings was determined by atomic force microscopy (AFM) to be between 40–60 nm. The peak thickness of the stamped film is about 70 nm. A minimum thickness can be ensured by spin-coating a thin PEDOT–PSS film on the substrate before stamping an additional PEDOT–PSS layer.

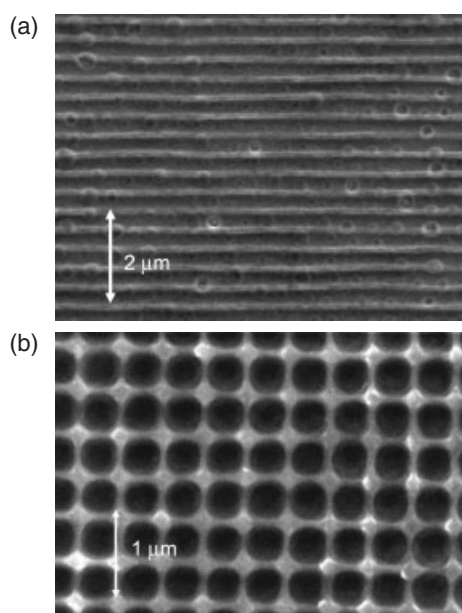


Figure 3. Scanning electron microscope (SEM) images of a) one-dimensional and b) two-dimensional gratings in a thin PEDOT film. The small circular defects in (a) were caused by microbubbles in the PDMS stamp. The bubbles can be avoided by placing the PDMS solution under vacuum before curing. This produces defect-free films as shown in (b).

2.3. Effect of Bragg Grating on LED Emission

Outcoupling from LEDs with one-dimensional stamped gratings was confirmed by collecting narrow-angle electroluminescence spectra. The narrow-angle (collection angle of 1°) s-polarized spectra shown in Figure 4a contain sharp peaks that correspond to grating outcoupling of waveguided light. The peak splitting occurs because the grating scatters waveguided light traveling in opposite directions.^[10] The propagation constants of the outcoupled waveguide modes can be calculated by inputting the peak wavelengths and collection angles to Equa-

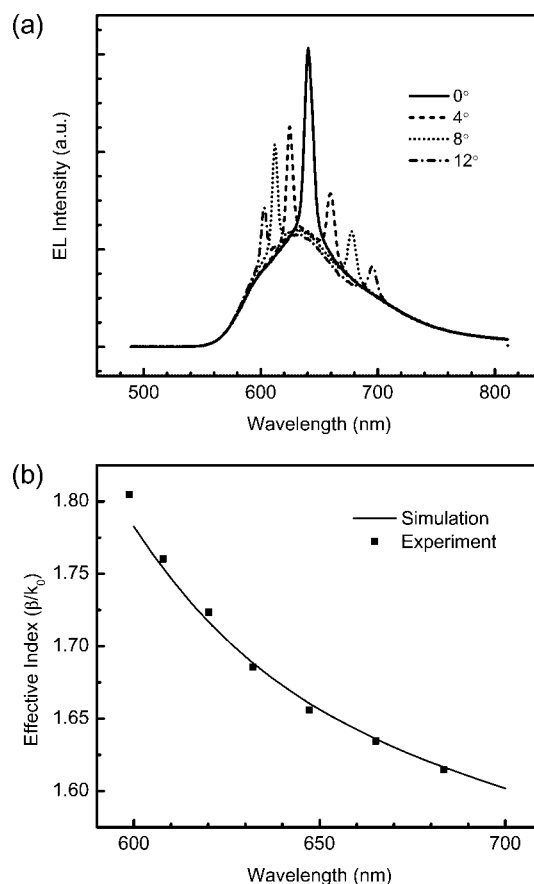


Figure 4. a) Angularly resolved s-polarized electroluminescence spectra from an LED show strong peaks that correspond to the outcoupling of waveguided light. This particular LED had a 270 nm thick active layer and a grating period $\Lambda = 375$ nm. b) The empirical waveguide modes calculated from the peak wavelengths for a 220 nm thick LED with a $\Lambda = 375$ nm grating show very good agreement with the numerical modeling results for the same LED structure without a grating.

tion 1. In Figure 4b the measured mode values are plotted along with the values calculated numerically. The strong agreement between the experimental and theoretical values confirmed that the sharp peaks arise from extraction of waveguided light. Further evidence for outcoupling by the Bragg grating was obtained by collecting p-polarized spectra. These spectra did not contain sharp peaks. This is expected since the LED is too thin to support transverse magnetic (TM)-polarized waveguide modes.

The effect of the grating on forward emission was observed by collecting electroluminescence spectra from the forward emission cone between $\pm 12^\circ$ from normal emission from the substrate. The relative enhancement of the grating is shown in Figure 5, which compares the emission spectra of a device with a grating to the emission spectra of a reference sample. This figure illustrates the increase in external emission due to the grating, as well as a slight change in the shape of the emission spectrum. The change in spectral shape is very strong near the vertical emission peak of the grating. In this case, vertical emission ($\theta = 0^\circ$) occurs for $\lambda = 640$ nm. Another important observa-

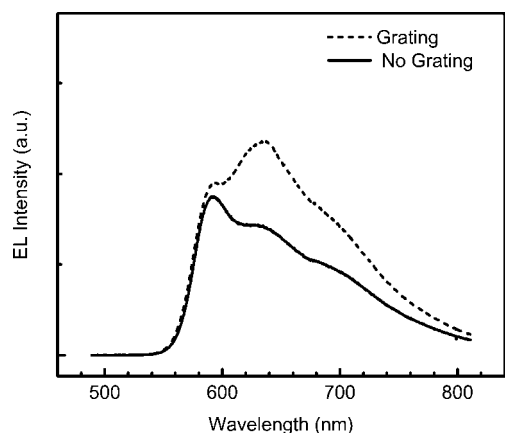


Figure 5. Comparison of forward emission (over the range of $\pm 12^\circ$) electroluminescence (EL) spectra for LEDs with and without a stamped grating. The active layer was 220 nm thick and the grating period was $\Lambda = 375$ nm.

tion is that the effect of the grating tends to decrease at shorter wavelengths due to the increase in absorption from the polymer film. In this case, the change in emission shape does not correspond to any significant shift in the color coordinates of the spectrum.

2.4. Effect of Polymer Thickness

The thickness of the polymer layer has a large effect on the waveguiding in the LED as shown in Figures 1,2. In this section, we demonstrate the effect this has on the coupling strength of the grating. An important effect of the polymer thickness for grating outcoupling is the intensity of the field at the interface between the PEDOT-PSS and the OC₁C₁₀-PPV. This is where the grating is located, so the higher the fields are at this interface the stronger the grating outcoupling will be. The field in the 100 nm thick device is not very strongly confined in the OC₁C₁₀-PPV and penetrates a large distance into the glass substrate; as a result the field intensity in the grating zone is low. In the 200 nm thick device, the waveguiding is much stronger, the mode is more confined, and the field intensity in the grating zone is higher. We have experimentally observed this effect by fabricating LEDs with varying active layer thicknesses. Figure 6 shows the enhancement of forward emission as a function of active layer thickness. It suggests that optimum outcoupling occurs when the active layer thickness is about 200 nm. Above 200 nm, the waveguide mode is strongly waveguided in the active layer but the field intensities and grating outcoupling are weaker because the overall waveguide is much thicker.

2.5. Effect of Waveguide Absorption

The field intensities in Figure 2 illustrate that the power in the waveguide modes penetrates evanescently into the clad-

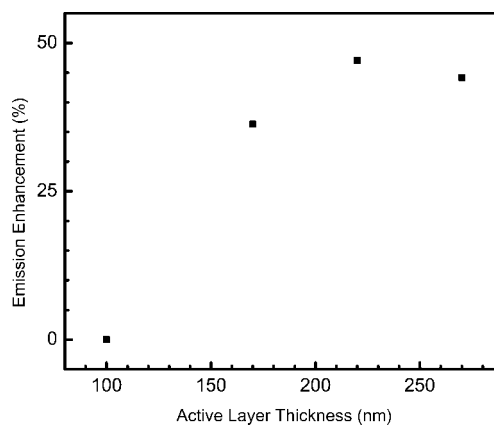


Figure 6. The emission enhancement in the forward direction (over the range of $\pm 12^\circ$) for LEDs with one-dimensional gratings with periods $\Lambda = 375$ nm versus active layer thickness. The enhancement was calculated by comparing the emission spectra with and without a grating for devices with identical thicknesses and integrating over all wavelengths.

ding regions. The ITO, PEDOT-PSS, calcium, and silver layers contain a large portion of the waveguided power and the localization of power in these regions leads to absorption of the waveguided light. We have calculated the decay length to be less than 5 μm throughout the emission spectrum of the LED. This absorption limits the number of grating periods that the waveguided light may interact with and limits the amount of light outcoupled by the grating.

The effect of waveguide absorption can be clearly seen from the photoluminescence spectra in Figure 7, which were performed on PEDOT-PSS gratings identical to those used in the LEDs, but with no ITO, calcium, or silver layers. These measurements show much stronger outcoupling than was observed in Figure 5 for the standard LED structure. We concluded that the ITO, calcium, and silver absorb a large fraction of the waveguided light and this light absorption significantly limits the effect of the grating.

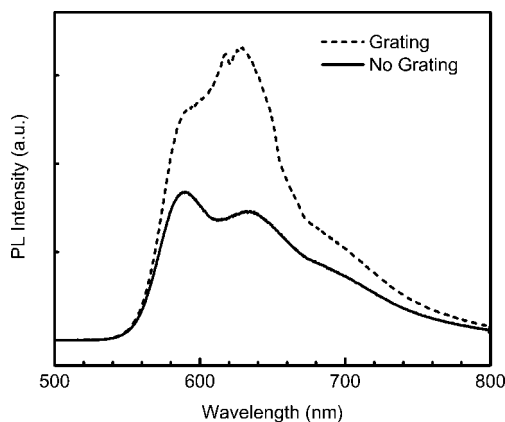


Figure 7. Comparison of forward emission (over the range of $\pm 12^\circ$) photoluminescence (PL) spectra for a bare 200 nm thick OC₁C₁₀-PPV film on a PEDOT film with and without a stamped grating. The grating period was $\Lambda = 375$ nm.

To minimize the effect of waveguide absorption on the efficiency of the grating, we varied the thickness of the calcium layer and observed a change in grating outcoupling. In Figure 8, we plot the grating outcoupling over the forward emission angles as a function of the thickness of the calcium layer.

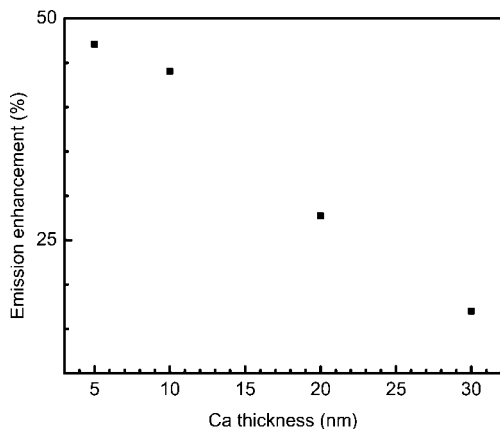


Figure 8. The variation in forward emission (over the range of $\pm 12^\circ$) with calcium thickness for LEDs with 200 nm thick active layers and one-dimensional gratings with periods $\Lambda = 375$ nm. The LED values were calculated by comparing the EL spectra to a reference LED and integrating over all wavelengths.

It shows a significant correlation between the outcoupling of the grating and the thickness of the calcium layer. This was caused by a change in the reflectivity of the metallic cathode. As we decreased the thickness of the calcium region, the optical properties of the cathode became more dependent on the properties of the silver layer. The high reflectivity of the silver pushes waveguide power out of the cathode, which causes high losses, and into the OC₁C₁₀-PPV region. This decreases waveguide absorption and increases the grating efficiency. In addition, more light diffracted by the grating into the cathode is reflected. The variation in calcium thickness did not affect the current–voltage characteristics of the LED as we decreased the calcium thickness to 5 nm. However, when we attempted to reduce the calcium thickness below 5 nm, we saw a significant increase in operating voltage and poor device performance.

2.6. Efficiency Enhancement

We have fabricated devices with optimum polymer and calcium thickness for grating outcoupling. In these devices, the active layer was 200 nm thick and the calcium layer was 5 nm thick. The effect of the stamped gratings on external quantum efficiency measured over all emission angles ($\pm 90^\circ$) is shown in Figure 9. One-dimensional gratings increased the efficiency by more than 15 % when compared to a reference LED. Two-dimensional crossed gratings increased the efficiency even further, emitting 25 % more light than the reference sample. The efficiency curves show that introducing the grating did not

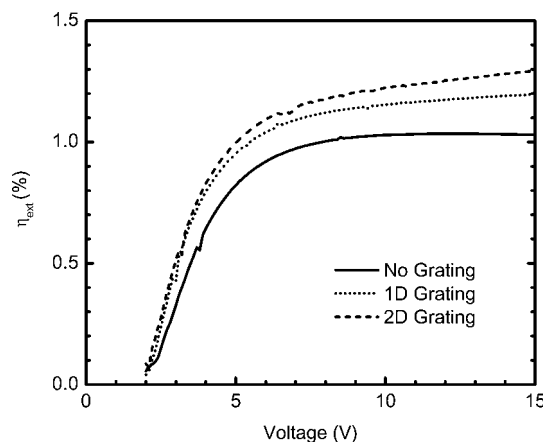


Figure 9. The external quantum efficiency (photons/electrons) of devices without a grating compared to devices with one and two-dimensional gratings versus applied voltage.

introduce any negative electronic effects, as the turn-on voltages remained unchanged. The external quantum efficiency values were relatively low because the polymer thickness was optimized for grating outcoupling and not for overall external quantum efficiency. It is important to note that the 15–25 % boost in external quantum efficiency corresponded to a 47–70 % increase in the forward directed emission measured over the range of $\pm 12^\circ$ from normal. The difference between the forward emission enhancement and the enhancement over all angles is due to the directionality of the outcoupling from the gratings. We report both values because there are some applications where only the forward directed emission is important and Bragg gratings are particularly useful.

3. Conclusions

In summary, we have demonstrated that gratings can be incorporated into polymer LEDs with a modified microtransfer molding technique. Using these gratings, we were able to increase the forward directed emission by 70 % and the external quantum efficiency by 25 %.

Our work has also revealed that competition between grating outcoupling and waveguide absorption is very important. When coupling is weak or waveguide absorption is large the efficiency of the grating is significantly reduced. There were two approaches for improving the efficiency of the grating: increasing the coupling coefficient of the grating and reducing the waveguide losses. By optimizing the thickness of the active polymer film, we were able to increase the coupling coefficient. In addition, we were able to reduce the waveguide loss by decreasing the thickness of the calcium layer. In the current structure, the optimum polymer thickness for outcoupling waveguided light is thicker than the optimum thickness for efficient recombination. In the future, we plan to investigate optimizing the location of the grating in the LED, reducing the waveguide absorption, and increasing the coupling coefficient.

4. Experimental

Modeling: The calculation of waveguide modes, waveguide absorption, and electric field intensities was performed using a transfer-matrix technique that has been described in detail elsewhere [23]. For a given wavelength, the transfer-matrix program solved Maxwell's equations for the electric field throughout the LED structure as a function of the in-plane component of the k -vector. Waveguide modes were calculated by finding the in-plane propagation vector β for which the fields were "bound", i.e., fields decayed exponentially in the outside layers. The waveguide modes were first solved for using the real part of the permittivities for each layer. Then the solution was perturbed with the imaginary parts from each layer. After perturbation, β became a complex number. The real part of β corresponds to the propagation term and the imaginary part corresponds to the loss term $a/2$. We estimated the decay length as simply $1/a$. The perturbation approach was valid because the loss term (~ 1000 – 2000 cm^{-1}) was much smaller than the propagation term (~ 140000 – 180000 cm^{-1}).

To insure accuracy, the variation of the complex refractive indices with wavelength was calculated for all the device layers. To input the indices into the modeling program, data obtained from our own measurements, from optical models, or from the papers cited previously were fit to functions of the free-space wavelength λ in units of nanometers. These functions are listed below.

Glass: $n = 1.6685 - 6.028 \times 10^{-4} \lambda + 8.29442 \times 10^{-7} \lambda^2 - 4.01656 \times 10^{-10} \lambda^3$

ITO: $n = [1 - 2.7889 / (1.5376 \times 10^6 / \lambda^2 + 186 / \lambda + 8.0969 / (23.814 - 1.5376 \times 10^6 / \lambda^2 - i 1.0416 \times 10^3 / \lambda) + 115.943 / (50.41 - 1.5376 \times 10^6 / \lambda^2 - i 12.4 / \lambda))]^{1/2}$

PEDOT: $n = 0.43867 + 0.00538 \lambda - 8.72511 \times 10^{-6} \lambda^2 + 4.31767 \times 10^{-9} \lambda^3 + i (6.347040 \times 10^{-1} - 6.281886 \times 10^{-3} \lambda + 2.592634 \times 10^{-5} \lambda^2 - 5.680962 \times 10^{-8} \lambda^3 + 6.962184 \times 10^{-11} \lambda^4 - 4.475634 \times 10^{-14} \lambda^5 + 1.173202 \times 10^{-17} \lambda^6)$

OC₁C₁₀-PPV: $n_{\parallel} = 31.58941 - 0.12317 \lambda + 1.70569 \times 10^{-4} \lambda^2 - 7.91257 \times 10^{-8} \lambda^3$

Calcium: $n = 0.35697 + 5.45016 \times 10^{-4} \lambda - 1.25436 \times 10^{-7} \lambda^2 + i(-0.4728 + 0.0052 \lambda - 8.18429 \times 10^{-7} \lambda^2)$

Silver: $n = (1 - 4.9039 \times 10^{-5} \lambda^2 + i 1.7942 \times 10^{-9} \lambda^3)^{0.5}$

Note that the OC₁C₁₀-PPV function describes only the in-plane refractive index, which is all that is needed for calculating TE modes.

Grating Fabrication: Grating templates were fabricated using holographic lithography with 400 nm thick films of Shipley S1805 resist and the 325 nm line from a helium-cadmium (HeCd) laser. Two-dimensional gratings were created by rotating the substrate 90° and repeating the exposure. Stamps were made by pouring Sylgard 184-PDMS, which was purchased from Fisher Scientific, over the master. The PDMS was cured at 100 °C for 2 h and removed from the master. The results reported in this paper were obtained with Bayer VP Al 4083 PEDOT-PSS that was purchased from H.C. Starck. The PEDOT-PSS was filtered before stamping using a 0.45 μm poly(vinylidene fluoride) (PVDF) filter.

LED Fabrication: LED fabrication was completed by spin-coating OC₁C₁₀-PPV films from a 1,2-dichlorobenzene solution followed by thermal evaporation of calcium and 30 nm of silver. The thickness of the calcium was monitored during deposition with a quartz crystal thickness monitor. The devices were encapsulated using glass and UV-cured epoxy so that measurements could be performed in air.

Luminescence Measurements: Angularly resolved electroluminescence measurements were carried out with an iris in front of the collection optics of a grating monochromator equipped with a polarizing filter and a charge coupled device (CCD) camera. The detected angle of emission was varied by rotating the LEDs. The angular resolution

was determined by the LED size, the distance from the LED to the iris and the diameter of the iris. In our measurements, it was less than 1°. Forward-emission measurements were performed by removing the iris and using the normal collection optics. In these measurements, the LED was oriented so that the emission would be collected from -12° to 12°. Photoluminescence was obtained by pumping with the 442 nm line of a HeCd laser. All electroluminescence spectra were recorded at a fixed current density of 20 mA cm⁻² using a Keithley 2400 source meter.

Efficiency Measurements: External efficiencies were obtained by collecting the emission from the LEDs with an integrating sphere. The emission was either collected by an optical fiber and coupled into a spectrometer or measured with a calibrated photodiode. The entire system was spectrally calibrated with a calibrated light source. Blackening the edges of the substrate eliminated emission from the sides and back of the glass substrates.

Received: October 1, 2003

Final version: November 23, 2003

- [1] J. S. Kim, P. K. H. Ho, N. C. Greenham, R. H. Friend, *J. Appl. Phys.* **2000**, *88*, 1073.
- [2] J. Gruner, R. Cacialli, R. H. Friend, *J. Appl. Phys.* **1996**, *80*, 207.
- [3] R. H. Jordan, L. J. Rothberg, A. Dodabalapur, R. E. Slusher, *Appl. Phys. Lett.* **1997**, *69*, 1997.
- [4] M. H. Lu, J. C. Sturm, *Appl. Phys. Lett.* **2001**, *78*, 1927.
- [5] C. F. Madigan, M. H. Lu, J. C. Sturm, *Appl. Phys. Lett.* **2000**, *76*, 1650.
- [6] T. Tsutsui, M. Yahiro, H. Yokogawa, K. Kawano, M. Yokoyama, *Adv. Mater.* **2001**, *13*, 1149.
- [7] T. Yamasaki, K. Sumioka, T. Tsutsui, *Appl. Phys. Lett.* **2000**, *76*, 1243.
- [8] H. Riel, S. Karg, T. Beierlein, B. Ruhstaller, W. Riess, *Appl. Phys. Lett.* **2003**, *82*, 466.
- [9] B. J. Matterson, J. M. Lupton, A. F. Safonov, M. G. Salt, W. L. Barnes, I. D. W. Samuel, *Adv. Mater.* **2001**, *13*, 123.
- [10] J. M. Lupton, B. J. Matterson, I. D. W. Samuel, *Appl. Phys. Lett.* **2000**, *77*, 3340.
- [11] Y.-J. Lee, S.-H. Kim, J. Huh, G.-H. Kim, Y.-H. Lee, S.-H. Cho, Y.-C. Kim, Y. R. Do, *Appl. Phys. Lett.* **2003**, *82*, 3779.
- [12] Y. R. Do, Y.-C. Kim, Y.-W. Song, C.-O. Cho, H. Jeon, Y.-J. Lee, S.-H. Kim, Y.-H. Lee, *Adv. Mater.* **2003**, *15*, 1214.
- [13] Y. Xia, G. Whitesides, *Annu. Rev. Mater. Sci.* **1998**, *28*, 153.
- [14] Y. Cao, I. D. Parker, G. Yu, C. Zhang, A. J. Heeger, *Nature* **1999**, *397*, 414.
- [15] J. M. Ziebarth, M. D. McGehee, *Appl. Phys. Lett.* **2003**, *83*, 5092.
- [16] C. M. Ramsdale, N. C. Greenham, *Adv. Mater.* **2002**, *14*, 212.
- [17] L. Pettersson, S. Ghosh, O. Inganas, *Org. Electron.* **2002**, *3*, 143.
- [18] M. Losurdo, M. Giangregorio, P. Capezzuto, G. Bruno, R. D. Rosa, F. Roca, C. Summonte, J. Pla, R. Rizzoli, *J. Vac. Sci. Technol. A* **2002**, *20*, 37.
- [19] M. Cavallini, M. Murgia, F. Biscarini, *Nano Lett.* **2001**, *1*, 193.
- [20] T. Granlund, T. Nyberg, L. Roman, M. Svensson, O. Inganas, *Adv. Mater.* **2000**, *12*, 269.
- [21] J. R. Lawrence, P. Andrew, W. L. Barnes, M. Buck, G. A. Turnbull, I. D. W. Samuel, *Appl. Phys. Lett.* **2002**, *81*, 1955.
- [22] J. Wang, X. Sun, L. Chen, S. Chou, *Appl. Phys. Lett.* **1999**, *75*, 2767.
- [23] J. Chilwell, I. Hodgkinson, *J. Opt. Soc. Am. A* **1984**, *1*, 742.